Int. J. Radiation Oncology Biol. Phys., Vol. 74, No. 3, pp. 844–851, 2009

0360-3016/09/$–see front matter

ELSEVIER

doi:10.1016/j.ijrobp.2008.09.026

CLINICAL INVESTIGATION **Radioimaging**

PELVIC LYMPH NODE TOPOGRAPHY FOR RADIOTHERAPY TREATMENT PLANNING FROM FERUMOXTRAN-10 CONTRAST-ENHANCED MAGNETIC RESONANCE IMAGING

Robert Dinniwell, M.D.,[*§††] Philip Chan, M.B.B.S.,[*§††] Gregory Czarnota, Ph.D, M.D.,[§#**] Masoom A. Haider, M.D.,[†‖] Kartik Jhaveri, M.D.,[†‖] Michael Jewett, M.D.,[‡¶] Anthony Fyles, M.D.,[*§††] David Jaffray, Ph.D.,[*§#] and Michael Milosevic, M.D.[*§††]

[*]Radiation Medicine Program, [†]Medical Imaging, and [‡]Surgical Oncology, Princess Margaret Hospital/Ontario Cancer Institute, University Health Network, Toronto, Canada; and Departments of [§]Radiation Oncology, [‖]Medical Imaging, [¶]Urology, and [#]Medical Biophysics, [**]Sunnybrook Health Sciences Centre, and [††]Institute of Medical Science, University of Toronto, Toronto, Canada

Purpose: To define a population-based pelvic lymph node clinical target volume (CTV) for radiotherapy treatment planning using magnetic resonance (MR) imaging and the ultrasmall superparamagnetic iron oxide lymph node contrast agent ferumoxtran-10.

Methods and Materials: A total of 55 eligible patients with endometrial, cervical, prostate, or bladder cancer underwent MR imaging sessions before and after contrast administration on 2 consecutive days. Ferumoxtran-10 was administered immediately after the first scan. The three-dimensional spatial distribution of the pelvic lymph nodes was determined in relation to adjacent vessels and other musculoskeletal landmarks, from which guidelines for determining a nodal CTV in individual patients were developed.

Results: On average, 30 lymph nodes (range, five to 62 nodes) were identified in each patient. The distribution of nodal distances to the closest artery or vein was observed to vary in different anatomic regions. Symmetrical three-dimensional margins of expansion around the distal para-aortic (12 mm), common iliac (10 mm), external iliac (9 mm), and internal iliac (10 mm) vessels, drawn in continuity with a 12-mm expansion anterior to the sacrum and a 22-mm expansion medial to the pelvic sidewall, were shown to encompass the majority of detectable lymph nodes in most patients.

Conclusion: Use of MR lymphography with ferumoxtran-10 provides an objective description of lymph node locations for radiotherapy planning. Use of this nodal CTV model in clinical practice could ensure a high probability of encompassing the regions at risk of harboring metastatic disease while minimizing the dose to adjacent normal tissues.

Cancer, Lymph node, Radiotherapy, Ultrasmall superparamagnetic iron oxide (USPIO), Ferumoxtran-10, Magnetic resonance (MR).

INTRODUCTION

Lymph node metastases are a common site of spread in patients with pelvic malignancies. Patients with a pelvic primary tumor and lymph node metastases at diagnosis have a significantly worse prognosis compared with those with no evidence of lymphatic involvement. Metastases to local and distant lymph nodes have a major role in tumor staging, therapy, and prognosis. Improvements in image-guided intensity-modulated radiotherapy (IMRT) treatment planning and delivery may help overcome the adverse prognostic significance of locoregional lymph node metastases and contribute to improved patient outcome.

A barrier to widespread implementation of IMRT for patients with pelvic malignancies is the absence of an objective description of lymph node locations in three-dimensional (3D) space that is used easily for radiation treatment planning. Conventional computed tomography (CT) and magnetic resonance (MR) do not reliably detect small pelvic lymph nodes, whether normal or abnormal, and have low sensitivity for identifying metastases, particularly in nodes less than 10 mm in the short-axis dimension

Reprint requests to: Michael Milosevic, M.D., F.R.C.P.C., Radiation Medicine Program, Princess Margaret Hospital, 610 University Avenue, Toronto, Ontario, Canada M5G 2M9. Tel: (416) 946-6522; Fax: (416) 946-6566; E-mail: mike.milosevic@rmp.uhn.on.ca

Supported by an ACURA Grant from the Canadian Association of Radiation Oncology; Canadian Prostate Cancer Research Initiative; Giovanni and Concetta Guglietti Family Trust; and in part by Varian Medical and the Susan Grange Family.

Conflict of interest: none.

Acknowledgments—The authors acknowledge the important contributions of Dr. Mukesh G. Harisinghani, Department of Abdominal Imaging, Massachusetts General Hospital; Ami Syed; and Anna Kirilova.

Received July 30, 2008, and in revised form Sept 18, 2008. Accepted for publication Sept 23, 2008.

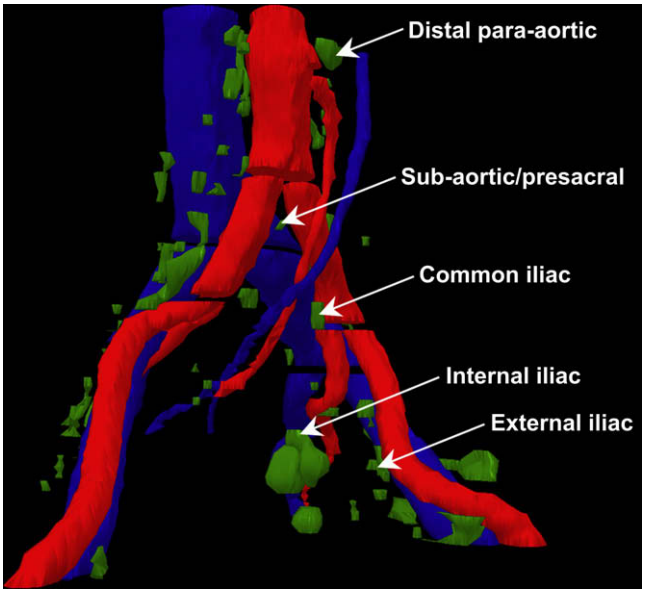

Fig. 1. Three-dimensional surface rendering of the contoured pelvic lymph nodes identified using ferumoxtran-10 in relation to the pelvic vasculature for a typical patient. Arteries indicated in red; veins, in blue; and lymph nodes, in green.

(1–4). Anatomic and embryologic studies have shown the close developmental and spatial relationships between the lymphatics and vasculature (5). The pelvic vessels are readily detected by using contrast-enhanced CT or MR and have been advocated as surrogates for lymph node location during treatment planning (6, 7). However, detailed information about the spatial distribution of nodal tissue in relation to the vessels at different anatomic levels in the pelvis is lacking.

Dextran-coated ultrasmall superparamagnetic iron oxide particles (USPIOs) have been evaluated as MR lymph node contrast agents for discriminating between malignant and benign lymph nodes (8–10). Although USPIOs have the potential to improve the identification of lymph node metastases in patients with pelvic malignancies relative to standard CT and/or MR techniques, it is unlikely that USPIOs will be able to identify microscopic nodal metastases with the accuracy of surgical staging (11). However, USPIOs have been shown to facilitate the identification of normal pelvic lymph nodes relative to CT or unenhanced MR (12). The improved identification of these nodes by using USPIOs and MR offers the potential of defining patient-specific nodal clinical target volumes (CTVs) in a minimally invasive manner that accounts for the risk of microscopic disease that cannot be imaged.

The aims of this study were to: (1) construct a high-quality nodal atlas describing probability distributions for normal and diseased pelvic lymph node number, size, and position based on a 55-patient sample; and (2) define the potential 3D nodal CTVs to be irradiated and a means of accurate delineation of these volumes in a 3D representation.

METHODS AND MATERIALS

Patient characteristics

The 55 patients included in this prospective study had a biopsy-proven pelvic malignancy. Median patient age was 62 years (range, 48–80 years). There were 12 women and 43 men (36 prostate cancers, nine bladder cancers, five endometrial cancers, and five cervical cancers). None had previously undergone pelvic lymph node dissection or received radiotherapy or chemotherapy. The study was approved by the Research Ethics Board of the University Health Network, Toronto, Canada, and written informed consent was obtained. Results of the study were not used in therapeutic decision making for these patients.

MR imaging

The MR was performed using a 1.5-Tesla magnet (GE Excite 1.5 T; Waukesha, WI) with a four-channel pelvic phased-array coil. Patients were instructed to take nothing by mouth 4 hours before the study. No other preparation was undertaken.

Axial imaging sequences were obtained 24–36 hours after contrast administration at 3-mm intervals through the pelvis. Pulse sequences consisted of T2-weighted Fast Spin Echo (repetition time/echo time/TE 6,500/80; field of view, 24–28 cm) and T2-star weighted dual-echo Gradient Recalled Echo (repetition time/echo time/TE1/TE2, 1,400/14/21 ms; field of view, 26–28 cm). Motion artifacts from peristalsis were minimized with the administration of hyoscine-*N*-butylbromide (Buscopan, Boehringer Ingelheim Ltd., Burlington, Canada), 30 mg, or glucagon, 1 mg, intravenously or intramuscularly before each MR imaging session.

Ferumoxtran-10

Ferumoxtran-10 (combidex, AMAG Pharmaceuticals Inc., Lexington, MA) was reconstituted from a lyophilized powder. A dose of 2.6 mg Fe/kg was dissolved in 100 ml of normal saline (0.9% sodium chloride) and infused intravenously.

Image analysis

Analysis of the Digital Imaging and Communications in Medicine images before and after contrast infusion was performed using 3D-DOCTOR (Able Software Corp., Lexington, MA). The lymph nodes, pelvic vasculature, and musculoskeletal landmarks for the subaortic/presacral space and obturator fossa/lateral pelvic sidewall were manually delineated by a single observer (R.D.) and reviewed by a radiologist. Voxels defining the edge of each distinct vessel and node were identified in the x and y planes for each axial slice (z plane). The x-y-z coordinates defining the segmented structures were then used to generate a 3D stacked image model.

Vascular segmentation

Segmentation of the pelvic arterial and venous system was performed in a caudal direction beginning from the abdominal aorta at the origin of the inferior mesenteric artery. At bifurcations, the first axial section that did not contain a part of the ''mother vessel'' was described as the beginning of the ''daughter vessel.'' The paired external iliac artery and vein were delineated inferiorly to the level at which the inguinal ligament traversed the medial aspect of the artery. To ensure consistency among patients, segmentation of these structures was continued to the superior aspect of the femoral heads in all cases.

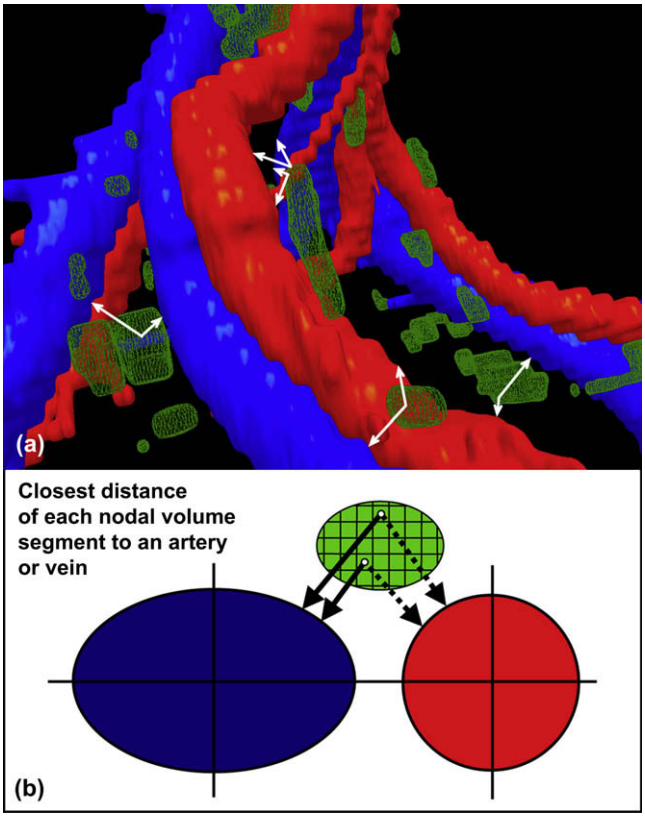

Fig. 2. (a) Three-dimensional surface rendering of the contoured pelvic lymph nodes and (b) a schematic representation of the method used to determine the spatial distribution of lymphatic tissue. The distance from the center of each lymph node volume unit (green) to the closest artery (red) and vein (blue) was calculated in three dimensions.

Lymph node nomenclature and segmentation

After administration of ferumoxtran-10, lymph nodes were detected by a decrease in signal on the dual gradient-echo images. Lymph nodes were classified into anatomic groups according to the following definitions, as shown in Fig. 1.

Distal para-aortic. Adjacent to the aorta and inferior vena cava from the inferior mesenteric artery to the bifurcation of these vessels.

Common iliac. Adjacent to the common iliac vessels from the aortic bifurcation to the branching of the internal iliac artery.

External iliac. Adjacent to the external iliac vessels inferior to the origin of the deep inferior epigastric vessels, extending anterior to the iliopsoas muscle and posterior to include the obturator lymph nodes within the obturator fossa.

Internal iliac. Along the medial aspect of the internal iliac vessels.

Subaortic/presacral. Inferior to the sacral promontory over the midportion of the sacrum, medial to the sacral foramina, and posterior to the peritoneum and posterior rectal surface.

All visible lymph nodes in these regions were contoured regardless of size and whether they were judged to contain metastatic disease.

Musculoskeletal boundary nomenclature and segmentation

Musculoskeletal landmarks were identified for the subaortic/presacral and pelvic sidewall lymph nodes. The subaortic/presacral landmark was the anterior aspect of the fifth lumbar vertebrae and sacrum from the bifurcation of the aorta and inferior vena cava superiorly to the inferior aspect of S3 and laterally to the sacral foramina. The pelvic sidewall landmark was the ilium/ischium and internal obturator muscle from the bifurcation of the common iliac vessels superiorly to the femoral canal inferiorly.

Table 1. Pelvic lymph node frequency and distribution

Vascular segment	No. of nodes		
	Total	Left	Right
Distal vena cava and para-aortic	1 (0–16)		
Common iliac	7 (0–20)	3 (0–10)	3 (0–10)
External iliac	11 (1–19)	5 (1–10)	5 (0–10)
Internal iliac	5 (0–15)	1 (0–8)	3 (0–7)
Subaortic/presacral	2 (0–6)		

Values expressed as median (range).

Measure of proximity of lymph nodes to vascular segments

To generate a complete 3D spatial representation of lymphatic tissue in each nodal segment, individual lymph nodes were first divided into small subunits measuring 0.5 (x axis) × 0.5 (y axis) × 3 (z axis) mm by using an automated algorithm (Fig. 2). Each subunit represented 0.75 mm^3 of lymphatic tissue. Distances in three dimensions from the center of each nodal subunit to the closest vascular edge (arterial or venous) were then calculated and grouped by vascular segment. Subaortic/presacral lymph nodes and iliac lymph nodes along the lateral pelvic sidewall were also localized in relation to musculoskeletal landmarks in the same manner. Histograms were generated for each vascular segment to illustrate the spatial distribution of nodal tissue in relation to the vessels or bony landmarks. Summary statistics were derived from the histograms to determine the vascular expansions required in each segment to encompass 50%, 80%, 90%, 99%, and 100% of lymphatic tissue.

RESULTS

Lymph node frequency, size, and location

A total of 1,670 lymph nodes defined by 5,663 separate nodal contours were detected in the 55 patients. The median number of lymph nodes was 30, with a range of five to 62 nodes (mean, 30 ± 12.8 [SD] nodes). For lymph nodes smaller than the chosen radiographic size criterion for metastasis (>10 mm), median short-axis size was 4 mm, with a range of 2–10 mm (mean, 3.7 ± 1.2 mm). Median total nodal volume was 6,650.0 mm^3 (range, 760.6–31,946.9 mm^3), and mean was 7,532.0 ± 5,569.9 mm^3. Table 1 lists the frequency distribution of lymph nodes in each vascular segment. Nodes were relatively uniformly distributed in the common iliac, external iliac, and internal iliac regions, but were less frequently detected in the subaortic/presacral and distal para-aortic regions. There were no significant differences in nodal frequency, size, or volume between the left and right sides of the pelvis or between men and women.

The main purpose of this study is to define lymph node target volumes for radiotherapy. Based on previous reports, it is unlikely that MR image enhancement with ferumoxtran-10 will allow lymph node metastases less than 3 mm to be detected reliably (11, 13). Therefore, radiotherapy target volumes will need to encompass all lymph nodes and not just

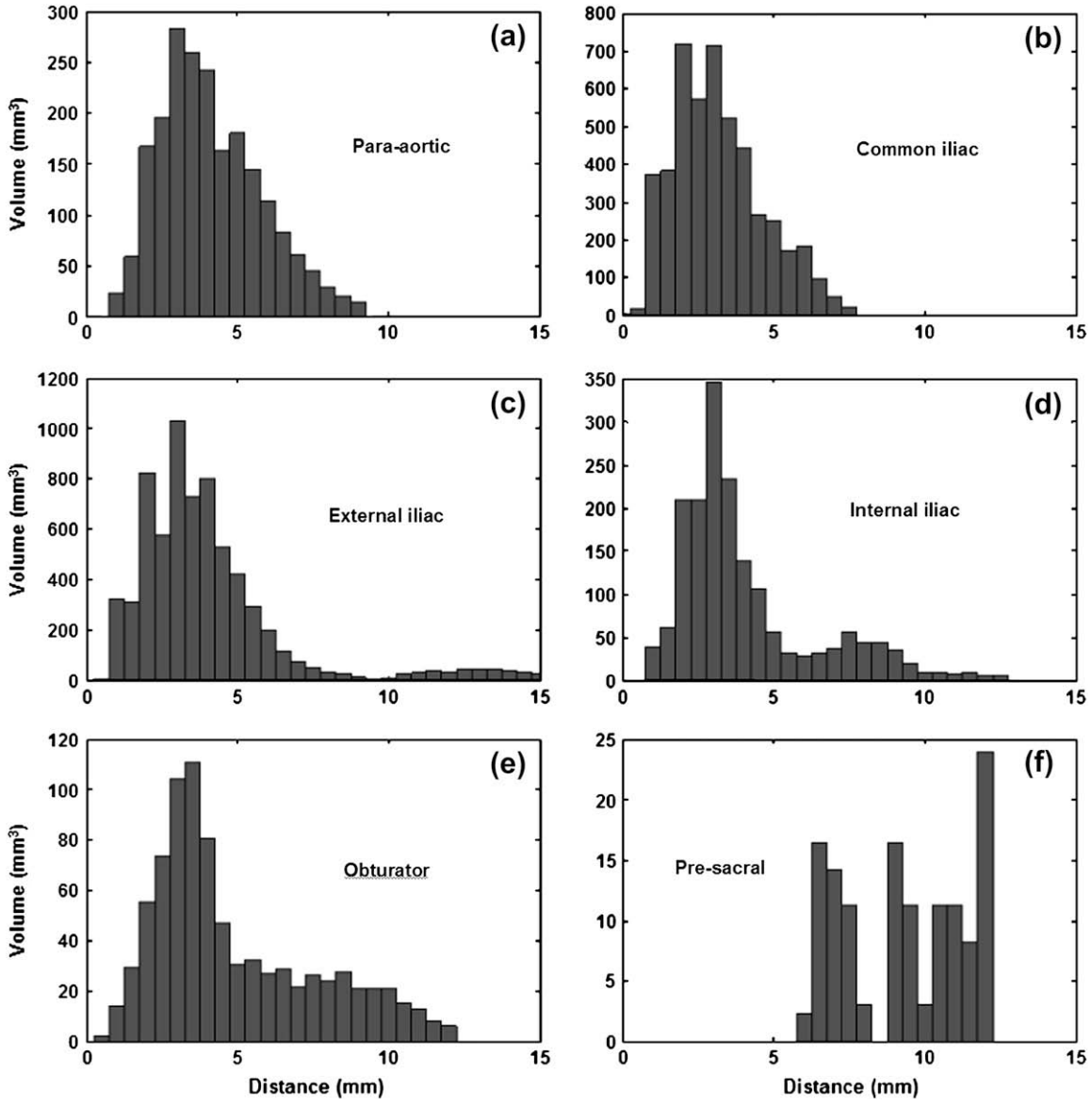

Fig. 3. Histograms for a typical patient show the spatial distribution of nodal tissue in relation to the closest edge of the nearest artery or vein in each anatomic nodal region: (a) distal para-aortic, (b) common iliac, (c) external iliac, (d) internal iliac, (e) pelvic sidewall, and (f) subaortic/presacral. Note the different Y axis scales reflecting differences in total lymphatic nodal volume from one region to another.

those with imaging evidence of metastatic disease. In addition, lymph nodes that were enlarged and at high risk of harboring metastatic disease according to commonly accepted CT and MR size criteria (short-axis diameter > 10 mm) were excluded from the histogram analysis to avoid biasing the results. This resulted in the removal of seven lymph nodes from the analysis in 4 patients (four left internal iliac, one right common iliac, one right external iliac, and one right external iliac node) and represented less than 0.5% of the total number of nodes identified.

Quantitative distance histogram analysis of lymph node volume

Lymph nodes in each patient were analyzed as a function of distance from the closest vessel. Figure 3 shows representative histograms from a typical patient for each vascular region. The small branches of the internal iliac vasculature in the presacral region were not consistently visualized on MR. Therefore, subaortic/presacral lymphatic tissue was related to the closest aspect of the anterior sacrum rather than the nearest visible vessel to avoid biasing results toward unusually long distances. For the same reason, obturator and medial internal iliac lymphatic tissue along the pelvic sidewall was related to the pelvic sidewall, as previously described (see Methods and Materials).

Spatial distribution of nodal tissue for the 55 eligible patients is listed in Table 2. On average, 90% of lymph nodes were detected within 8.7 mm of the nearest vessel in the distal para-aortic region, 7.3 mm in the common iliac region, 10.1 mm in the external iliac region, and 12.1 mm in the internal iliac region. However, there was marked variability among patients.

Table 2. Spatial distribution of lymph node tissue in relation to the closest vessel in each vascular segment

	Distance of lymphatic tissue from nearest vessel (mm)					
Percentile	50%	80%	90%	95%	99%	100%
Distal para-aortic	4.8 (2.4–11.5)	7.6 (3.2–22.4)	8.7 (3.6–23.2)	9.4 (3.7–23.9)	10.4 (4.0–24.6)	11.1 (4.0–24.8)
Common iliac	4.1 (2.1–10.5)	6.2 (2.8–18.8)	7.3 (3.1–20.9)	8.2 (3.3–21.9)	9.6 (3.5–23.1)	10.4 (3.8–23.9)
External iliac	5.2 (2.4–11.5)	8.3 (3.1–14.7)	10.1 (3.4–17.4)	11.5 (3.7–19.4)	14.0 (4.2–22.9)	15.8 (4.2–26.9)
Internal iliac	7.0 (2.8–20.3)	10.0 (3.3–27.2)	12.1 (3.4–29.8)	13.2 (3.4–30.6)	14.7 (3.4–31.8)	15.0 (3.4–32.4)
Subaortic/presacral*	15.5 (3.6–31.1)	19.9 (5.1–36.9)	20.5 (5.9–37.7)	20.8 (6.4–38.1)	21.2 (6.7–38.6)	21.3 (6.9–38.6)
Obturator*						

Values expressed as mean for the entire cohort (range in individual patients).
* Lymphatic tissue in each anatomic region was localized in relation to the closest artery or vein.

Although the distribution of nodal tissue along blood vessels was noted to be anisotropic and varied along the length of each relevant vascular segment, isotropic (uniform) margins of vascular expansion were assessed with the intent of generating a practicable method of 3D nodal CTV delineation.

The small vessels associated with the subaortic/presacral and obturator lymph nodes were not consistently visualized, and readily identifiable musculoskeletal landmarks were used instead. In the subaortic/presacral nodal region, mean distance anterior to the sacrum to encompass 90% of nodal tissue was 8.2 mm, and in the obturator region, mean distance from the pelvic sidewall to encompass 90% of the nodal tissue was 7.9 mm.

Nodal CTV for pelvic radiotherapy

The main objective of this study is to define clinically practicable rules for determining a lymph node CTV for patients receiving pelvic radiotherapy. The spatial distributions of lymph node tissue in relation to vascular or musculoskeletal landmarks listed in Tables 2 and 3 suggest that different margins of expansion around these anatomic surrogates may be optimal in different anatomic regions. The rules for nodal CTV delineation were derived by using 3D margins of expansion sufficient to cover 90% of the nodal tissue in 90% of patients. This definition was chosen as a compromise between nodal coverage and excessive normal tissue irradiation. The required margins of expansion around the distal para-aortic, common iliac, external iliac, and internal iliac vessels were 12, 10, 9, and 10 mm, respectively. In addition, a 22-mm medial expansion from the lateral pelvic sidewall, contiguous anteriorly and posteriorly with the expansions of the external and internal iliac vessels, respectively, was required to encompass the obturator and medial internal iliac lymph nodes. A 12-mm expansion was required anterior to the sacrum from S1–S3, contiguous laterally with the expansion of the iliac vessels, to encompass the subaortic/presacral nodes. Figure 4 shows the use of these guidelines to devise a nodal CTV for pelvic radiotherapy. The anatomic expansions were trimmed to exclude bone, muscle, and fascia, as well as bowel and bladder, because the space occupied by any of these tissues has a very low probability of also containing nodal tissue at either the time of imaging or later times (data not shown) (14, 15).

DISCUSSION

The lymphatic system is a prominent route of spread for many malignancies. Current imaging techniques are limited in their ability to reliably detect micrometastases in lymph nodes. Therefore, radiation treatment of apparently normal lymph nodes often is advocated as a means of improving local disease control and improving survival in patients with endometrial, cervix, bladder, prostate, and gastrointestinal cancer. The current evolution toward the use of high-precision IMRT to treat pelvic lymph nodes at risk of harboring occult disease demands accurate knowledge of the location of these nodes for target-volume definition. This study provides a comprehensive description of the spatial distribution of pelvic lymph nodes derived from MR imaging and the use

Table 3. Spatial distribution of lymph node tissue in relation to the closest vessel in each vascular segment and musculoskeletal land markers

	Distance of lymphatic tissue from nearest vessel or musculoskeletal land marker (mm)					
Percentile	50%	80%	90%	95%	99%	100%
Distal para-aortic	4.6 (2.4–1.5)	7.0 (3.2–17.7)	8.2 (3.6–19.8)	8.8 (3.7–20.9)	9.9 (4.0–22.4)	10.5 (4.0–23.8)
Common iliac	4.0 (2.1–10.4)	6.1 (2.8–18.8)	7.2 (3.1–20.9)	8.2 (3.2–21.9)	9.6 (3.5–23.1)	10.3 (3.8–23.9)
External iliac	3.9 (2.4–5.5)	5.5 (3.1–7.8)	6.6 (3.4–10.1)	7.6 (3.7–12.3)	9.4 (4.2–15.0)	10.9 (4.2–17.8)
Internal iliac	4.6 (2.8–8.4)	6.1 (3.3–11.0)	6.9 (3.4–13.5)	7.6 (3.4–14.5)	8.5 (3.4–15.6)	8.9 (3.4–16.6)
Subaortic/presacral*	6.0 (3.0–10.3)	7.8 (3.5–15.1)	8.2 (3.8–16.5)	8.5 (4.2–17.2)	8.8 (4.2–17.8)	8.9 (4.2–18.2)
Obturator*	4.6 (2.6–7.2)	7.1 (3.4–12.2)	7.9 (3.6–18.9)	9.8 (3.9–19.8)	11.8 (4.3–21.1)	13.3 (4.3–22.7)

Values expressed as mean for the entire cohort (range in individual patients).
* Lymphatic tissue in each anatomic region was localized in relation to the closest artery or vein, except in the subaortic/presacral and obturator regions, where it was related to musculoskeletal land markers (see text).

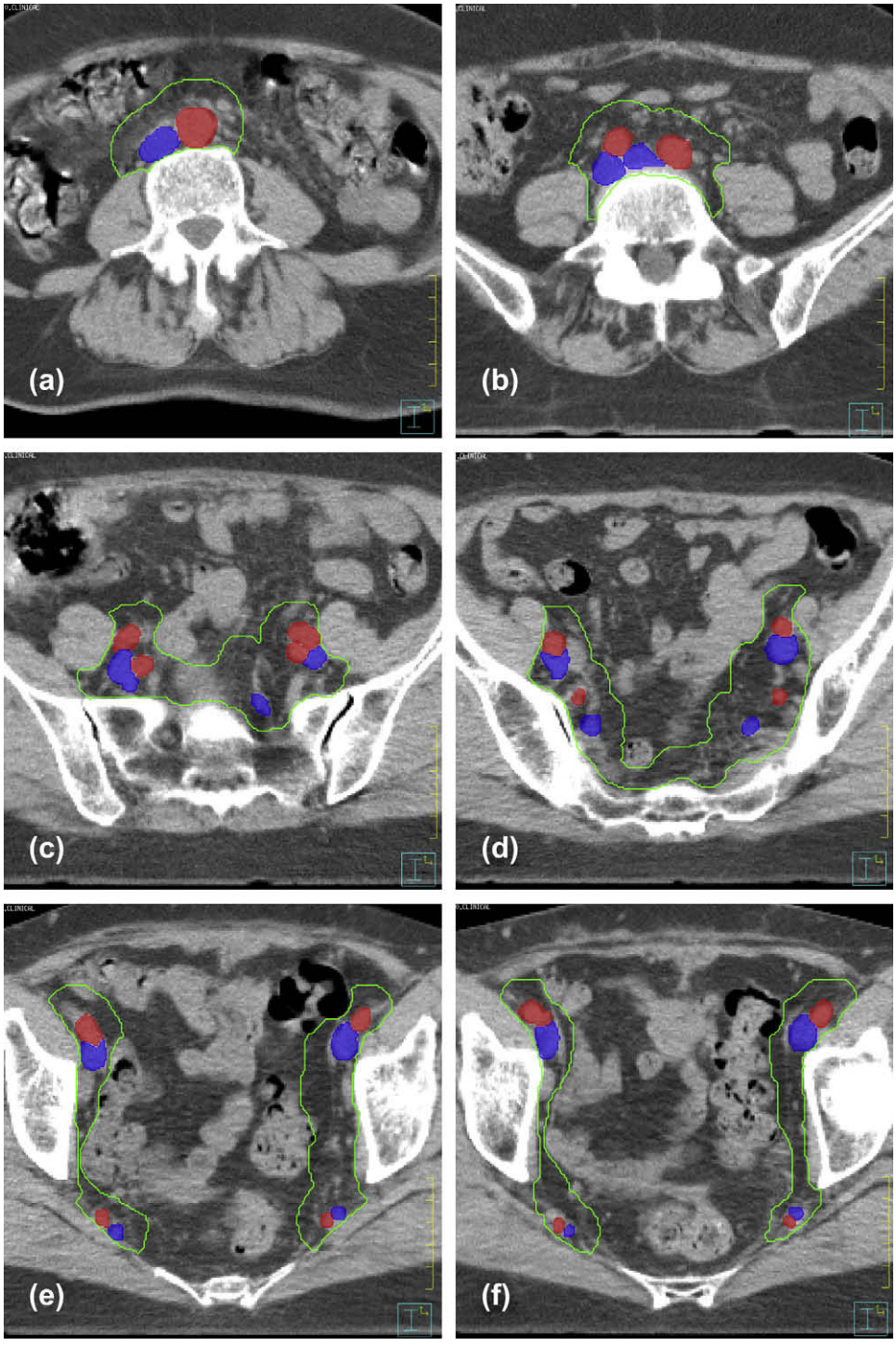

Fig. 4. Pelvic nodal clinical target volume at six craniocaudal levels in the pelvis developed by using our population-based model of lymph node tomography. Vascular, sacral, and pelvic sidewall expansions were trimmed to exclude bone, muscle, fascia, bladder, and bowel. (a) Distal para-aortic, (b) bifurcation of the aorta and inferior vena cava, (c) inferior to the bifurcation of the common iliac vessels, (d) midpelvis, (e) cranial to the acetabulum, and (f) acetabulum.

of a lymph node contrast agent in 55 patients. The results of this study show that: (1) ferumoxtran-10 subjectively enhances the capability of MR to detect pelvic lymph nodes regardless of whether involved by cancer; (2) for CTV definition, appropriate margins of expansion around major pelvic vessels or musculoskeletal nodal surrogates vary according to anatomic regions; and (3) the margins of expansion required around these anatomic surrogates to reliably encompass high-risk nodes are larger than advocated in previous studies (6). A population-based model of pelvic lymphatic topography has been presented, along with a set of clinically relevant rules for nodal target-volume definition.

This study, in agreement with others, shows that pelvic lymph nodes generally are situated close to vessels (5).

This was particularly evident in the distal para-aortic, common iliac, and external iliac regions, as shown in Fig. 3 for a representative patient and listed for the entire cohort in Tables 2 and 3. However, nodal tissue in the subaortic/presacral and obturator regions was found at greater distance from the major arteries and veins. These nodes are associated with smaller branches of the iliac vessels that are too small to be visualized reliably by using MR. Therefore, the major vessels alone do not provide sufficient surrogate information for lymph node CTV definition, and it was necessary to incorporate bony landmarks into our population-based model of nodal topography. The model suggests that 90% of nodal tissue in 90% of patients will be encompassed by symmetrical 3D expansions of the distal para-aortic (12 mm), common iliac (10 mm), external iliac (9 mm), and internal iliac (10 mm) vessels, drawn in continuity with a 12-mm expansion anterior to the sacrum and a 22-mm expansion medial to the pelvic sidewall, as shown in Fig. 4. The union of the major artery and vein contours should be used to form the nodal CTV, and the resultant volume should be trimmed to exclude bone, muscle, fascia, bladder, and bowel, consistent with other recommendations (14, 15). Although population-based models facilitate treatment planning, it is important to carefully review all relevant imaging for each patient and adapt the nodal CTV contours to encompass overt lymphadenopathy or nodal outliers.

There are at least two other descriptions of pelvic lymph node topography for radiotherapy treatment planning derived from MR imaging of ferumoxtran-10 (6, 7). Shih *et al*. (7) mapped the center of mass of lymph node metastases in 18 men with prostate cancer to a standardized 3D model using anatomic landmarks. A 2-cm uniform margin of expansion was found to encompass 94.5% of lymph nodes believed to be at risk of harboring disease, assuming a fixed nodal diameter of 1 cm. This margin of expansion probably is excessive based on our analysis of the spatial distribution of lymphatic tissue in 55 patients and would unnecessarily limit the utility of IMRT to spare adjacent normal tissues. Taylor *et al*. (6), in a series of 20 women with gynecologic tumors, found a 7-mm vessel expansion to be optimal provided that the contours were manually modified using specified rules to include potential nodal locations at greater distances from major arteries and veins. Despite the apparent difference in proposed margins of expansion between that study and ours, the derived nodal CTVs are similar. The manual contour modifications implicit in the CTV definition of Taylor *et al*. (6) in effect further expand their 7-mm vessel margins so that the final volumes are relatively coincident. Our approach may be less time consuming and less prone to error because less revision is required for individual cases.

The greatest limitation of this and previous studies is the ability of MR imaging with ferumoxtran-10 to identify small lymph nodes less than 3 mm and microscopic lymph node metastases. The nodes comprising the presacral and internal iliac groups likely are underrepresented by virtue of their size. Taylor *et al*. (6) reported the frequency of lymph node contours, and a summation of consecutive contours through successive axial images is required to determine the lymph node numbers identified for each lymph node group specified. Within their 20-patient series, a mean of 0.4 (range, none to two) and 7.2 (range, one to 22) lymph node contours were identified for the presacral and internal iliac lymph node groups, respectively. In comparison, a median of two (range, none to six) and five (range, none to 15) presacral/subaortic and internal iliac lymph nodes were identified in our 55-patient series. Recognizing that the presacral lymph node group in our series included subaortic lymph nodes and nodes within each group may lie across more than one adjacent axial plane, there would appear to be an equivalent or greater number of lymph nodes identified in our series with a larger sample size. Our model for nodal CTV definition was derived from the spatial distribution of visible lymph nodes on the assumption that these would be representative of all nodes at risk of harboring disease. It is possible that there are small lymph nodes at greater distances from the major vessels that were not visualized using this approach. However, these are likely to represent a small proportion of total nodal volume in each anatomic region and would not substantially alter the proposed margins of expansion, which were defined to encompass 90% of lymphatic tissue in 90% of patients. Ferumoxtran-10, while lowering the MR threshold for detection of subclinical disease, does not enhance sensitivity enough to reliably detect microscopic metastases (11). This currently limits the utility of this approach for defining patient-specific radiotherapy volumes that target only regions of known tumor. However, innovative cellular MR techniques using magnetic nanoparticles have been shown in preclinical studies to detect as few as 100 malignant cells in lymph nodes and hold great promise for the future (16).

In conclusion, the use of MR lymphography provides an objective 3D spatial description of relevant pelvic lymph nodes in relation to easily visualized anatomic landmarks. Radial 3D margins of expansion around the major pelvic vessels, with the inclusion of separate margins for the sacral and medial external and internal iliac lymph nodes, can be used to develop a population-based nodal CTV for radiotherapy treatment planning. Use of this model in clinical practice will ensure a high probability of encompassing most of the nodal tissue at risk of harboring metastases in most patients while minimizing the dose to normal tissues.

REFERENCES

1. Bipat S, Glas AS, van der Velden J, *et al*. Computed tomography and magnetic resonance imaging in staging of uterine cervical carcinoma: A systematic review. *Gynecol Oncol* 2003; 91:59–66.

2. Hacker A, Jeschke S, Leeb K, *et al*. Detection of pelvic lymph node metastases in patients with clinically localized prostate cancer: Comparison of [18F]fluorocholine positron emission tomography-computerized tomography and laparoscopic

radioisotope guided sentinel lymph node dissection. *J Urol* 2006;176:2014–2018. discussion; 2018–2019.
3. Golder WA. Lymph node diagnosis in oncologic imaging: A dilemma still waiting to be solved. *Onkologie* 2004;27:194–199.
4. Park JY, Kim EN, Kim DY, *et al*. Comparison of the validity of magnetic resonance imaging and positron emission tomography/computed tomography in the preoperative evaluation of patients with uterine corpus cancer. *Gynecol Oncol* 2008;108:486–492.
5. Viamonte MR. Atlas of lymphography. New York: Thieme-Stratton; 1980.
6. Taylor A, Rockall AG, Reznek RH, *et al*. Mapping pelvic lymph nodes: Guidelines for delineation in intensity-modulated radiotherapy. *Int J Radiat Oncol Biol Phys* 2005;63:1604–1612.
7. Shih HA, Harisinghani M, Zietman AL, *et al*. Mapping of nodal disease in locally advanced prostate cancer: Rethinking the clinical target volume for pelvic nodal irradiation based on vascular rather than bony anatomy. *Int J Radiat Oncol Biol Phys* 2005;63:1262–1269.
8. Tabatabaei S, Harisinghani M, McDougal WS. Regional lymph node staging using lymphotropic nanoparticle enhanced magnetic resonance imaging with ferumoxtran-10 in patients with penile cancer. *J Urol* 2005;174:923–927 discussion, 927.
9. Harada T, Tanigawa N, Matsuki M, *et al*. Evaluation of lymph node metastases of breast cancer using ultrasmall superparamagnetic iron oxide-enhanced magnetic resonance imaging. *Eur J Radiol* 2007;63:401–407.
10. Curvo-Semedo L, Diniz M, Migueis J, *et al*. USPIO-enhanced magnetic resonance imaging for nodal staging in patients with head and neck cancer. *J Magn Reson Imaging* 2006;24:123–131.
11. Li Z. Efficacy and safety of combidex (NDA 21-115). Available at: http://www.fda.gov/OHRMS/DOCKETS/ac/05/slides/2005-4095S1_02_01-FDA-Li.ppt. Accessed November 11, 2008.
12. Bellin MF, Lebleu L, Meric JB. Evaluation of retroperitoneal and pelvic lymph node metastases with MRI and MR lymphangiography. *Abdom Imaging* 2003;28:155–163.
13. Harisinghani MG, Barentsz J, Hahn PF, *et al*. Noninvasive detection of clinically occult lymph-node metastases in prostate cancer. *N Engl J Med* 2003;348:2491–2499.
14. Vilarino-Varela MJ, Taylor A, Rockall AG, *et al*. A verification study of proposed pelvic lymph node localisation guidelines using nanoparticle-enhanced magnetic resonance imaging. *Radiother Oncol* 2008;89:192–196.
15. Lawton CAF: Pelvic nodal consensus CTV contours: High risk/locally advanced adenocarcinoma of the prostate. Available at: http://www.rtog.org/PelvicLymphNodeProstateAtlas/main.html. Accessed November 11, 2008.
16. Foster PJ, Dunn EA, Karl KE, *et al*. Cellular magnetic resonance imaging: In vivo imaging of melanoma cells in lymph nodes of mice. *Neoplasia* 2008;10:207–216.